Soft Matter

Boronic acid-mediated mucin/surface interactions of zwitterionic polymer brushes

Journal:	*Soft Matter*
Manuscript ID	SM-ART-12-2024-001502.R2
Article Type:	Paper
Date Submitted by the Author:	18-Mar-2025
Complete List of Authors:	Cureno Hernandez, Karla; Colorado State University, School of Materials Science and Engineering Lee, Jeonghun; Colorado State University, School of Materials Science and Engineering Kim, Sunghoon; Colorado State University, School of Materials Science and Engineering Cartwright, Zachary; Colorado State University, School of Biomedical Engineering Herrera-Alonso, Margarita; Colorado State University, Chemical and Biological Engineering

Boronic acid-mediated mucin/surface interactions of zwitterionic polymer brushes

Karla E. Cureno Hernandez[1], Jeonghun Lee[1], Sunghoon Kim[1], Zach Cartwright[2], Margarita Herrera-Alonso[1,3]*

[1] School of Materials Science and Engineering, Colorado State University, Fort Collins, Colorado, 80523, United States

[2] School of Biomedical Engineering, Colorado State University, Fort Collins, Colorado, 80523, United States

[3] Department of Chemical and Biological Engineering, Colorado State University, Fort Collins, Colorado, 80523, United States

ABSTRACT

Mucus is a substance that acts as a protective barrier, shielding tissues from infections caused by viruses and bacteria. Recent studies highlight the advantages of transmucosal drug delivery compared to traditional delivery methods. However, external particles in mucus struggle to penetrate its deeper layers and are often eliminated by mucus clearance mechanisms, hindering effective drug delivery. To gain a deeper understanding of how material surfaces interact with mucus, we grafted brushes of poly(2-methacryloyloxyethyl phosphorylcholine) (PMPC) onto silica surfaces, followed by the straightforward installation of a terminal boronic acid moiety (3-phenylboronic acid, APBA). The modification process was carried out following a surface-initiated activator regenerated by electron transfer atom transfer radical polymerization (SI-ARGET ATRP), a method known for its effectiveness in producing well-defined grafted polymers. After conjugation of APBA, we studied the effects of surface chemistry on properties such as pH-sensitivity and mucin adsorption. The surfaces modified with the zwitterionic polymer showed no mucin interaction regardless of system pH. However, all the surfaces containing the boronic acid showed boronic acid-sialic acid interactions, particularly at lower pH values. The insights gained from this study will enhance our understanding of the interactions between the zwitterionic PMPC

and the boronic acid APBA with mucins, laying the groundwork for future chemical modifications of particle surfaces aimed at modulating their transport through mucus.

INTRODUCTION

Transmucosal drug delivery involves the administration of therapeutic agents through mucosal membranes, offering a non-invasive and highly patient-compliant alternative to traditional methods.[1] This approach allows for targeted delivery to specific organs via intranasal, oral, and rectal routes, while also minimizing or avoiding complex pathways.[2–4] One example of an efficient mucopenetrating system is the influenza A virus. It has been shown that the surface of the virus is decorated with the receptor-binding protein hemagglutinin (HA) and the receptor-cleaving enzyme neuraminidase (NA).[5] While HA is responsible for host cell recognition, NA prevents aggregation and entrapment of the virus in the mucosal membrane.[6] For an effective infection, the function of both HA and NA should be balanced. Therefore, changes in the activity of these two proteins must be followed by an adjustment of the activity of the other.[6–8]

Transmucosal delivery strategies are generally divided into two categories: mucoadhesive and mucopenetrating. Mucoadhesive methods focus on enhancing the retention of carriers at the mucosal site. These carriers typically possess hydrophobic properties, a positive charge, or functional groups that interact with mucus through mechanisms like van der Waals forces, hydrogen bonding, or dynamic covalent bonding.[9–13] Conversely, mucopenetration offers another approach to achieve effective transmucosal delivery. This strategy utilizes mucorepulsive interactions and focuses on creating formulations that enhance the residence time of carriers at specific mucosal sites by facilitating deeper penetration into the mucus. Research indicates that carriers capable of this deeper penetration are typically hydrophilic and electrically neutral.[14–16] Thus, both mucoadhesive and mucopenetrating carriers exhibit valuable characteristics for optimizing transmucosal drug delivery.

Poly(ethylene glycol) (PEG) has been the most widely used polymer for coating nanocarriers used for transmucosal delivery, demonstrating good transport through mucus.[16–19] PEG has been shown to repel protein adsorption thus preventing drug carriers from binding to the surface of mucus. Although this polymer has been referred to as the standard for mucopenetration, it is recognized that PEG suffers damage by oxidation in the presence of transition metals and oxygen present in

relevant biochemical solutions, and it also loses its protein repulsive properties above 35 °C.[16,18] Furthermore, there is increasing concern regarding accumulated toxicity and immunogenicity associated with PEG-based systems.[20–24]

Nanoparticles with zwitterionic polymer coatings have also shown excellent mucopenetrating characteristics.[25–27] Zwitterionic compounds are those bearing an equal number of anionic and cationic charges, but are net neutral.[20,28] It is also known that viruses can easily diffuse through mucus and their surface exhibits equal densities of positive and negative charges and the absence of hydrophobic patches.[14] By learning from nature, zwitterionic materials are used to enhance the mucus penetration of drug delivery vehicles. The most representative zwitterions are phosphorylcholine-, sulfobetaine- and betaine-based. These types of polymers are known to exhibit resistance to non-specific protein adsorption, which has favored their application as biosensors, surfaces resistant to bacterial adhesion and protein contamination. Furthermore, since their structure exhibits a significant dipole moment, zwitterionic polymers have been shown to have great stability under a wide range of salt concentrations, which has led to their relevance in biomedical applications such as glucose monitors, antibacterial coatings and blood purification devices.[29–31] These materials have been found to be bioinert and biocompatible with a superior hydrophilic surface, an important characteristic for mucopenetration. Interestingly, it has recently been shown that poly(carboxybetaine)-coated nanoparticles diffuse through mucus an order of magnitude faster than PEG-coated particles.[26,32,33]

Boronic acids (BA), on the other hand, have been of interest as materials for biomedical applications due to their biocompatibility, unique reactivity, and especially for their characteristic reversible interaction with diols. Among their most notable biomedical applications are materials used as biosensors, thermo- and saccharide-responsive hydrogels, targeted drug delivery, bioimaging, and treatment of HIV and diabetes.[34–37] Boronic acid-containing materials have also been shown to improve the effectiveness of mucoadhesive nanoparticles for drug delivery.[38] In aqueous solution, boronic acids exist in equilibrium between their neutral form and a hydroxyboronate anion. Similar to carboxylic acids, boronic acids can form esters, most frequently with 1,2- and 1,3-diols.[39–41] This characteristic allows the formation of boronate esters with several biologically important species, including sialic acids, abundant components in mucus. This interaction is known for its high reaction specificity, and its binding affinity is sensitive to chemical

structure and system pH.[39] Noteworthy examples of the use of boronic acids to improve the mucoadhesion of polymer-based materials include boronated chitosan for the controlled delivery of insulin,[42–45] for the development of membranes with targeted adhesion,[46] as polymer microneedle patches with antimicrobial properties,[47] for ocular drug delivery,[48] and as injectable hydrogels for endoscopic submucosal dissection.[49] Several examples of the synthesis and characterization of boronic acid-decorated particles have been reported to investigate their mucoadhesive properties and stability in media with varying pH.[34,46,50,51] However, to the best of our knowledge, no system exists that combines both functionalities to study how surface chemistry influences interactions with mucin.

Polymer brushes consist of polymer chains densely anchored onto the surface of a substrate, and have found widespread applications in a number of different fields including antifouling coatings, biosensing, catalysis, drug delivery, lubrication, tissue engineering, and ultrafiltration.[52–57] Although the initial approach to realizing polymer brushes was based on the "*grafting to*" method,[58–60] surface-initiated approaches are increasingly adopted as the methods of choice as they yield polymer brushes with higher grafting density, more uniformly consistent layers, and the ability to readily tailor end-group functionality. Surface-initiated atom transfer radical polymerization (SI-ATRP) methods have been developed to enable the growth of well-defined polymer brushes on a variety of substrates, and in this way achieve control over surface properties. In SI-ATRP, the organohalogen initiator is grafted onto the surface and the equilibrium between propagating and dormant species is regulated by the metal complex catalyst.[52] Various SI-ATRP strategies have evolved from the conventional SI-ATRP approach, including ARGET-ATRP (activators regenerated by electron transfer), SARA-ATRP (supplemental activators and reducing agents), eATRP (electrochemically mediated), and photo-ATRP (photoinduced).[61] We refer the reader to reviews highlighting examples of these and other SI-ATRP methods and their applications.[52–56,62,63] SI-ARGET ATRP evolved to expand the application range of SI-ATRP through the addition of a reducing agent to continuously regenerate the active form of the catalyst, thus requiring lower catalyst loading and increased oxygen tolerance.[53,64–66] This method has been useful for generating polymer brushes with pH- and oxidative-responsiveness,[67] for coating wood surfaces with hydrophobic and antibacterial coatings,[68] and for producing zwitterionic polymer coatings with antifouling[64,65,69,70] or blood compatible properties.[71]

To better understand the interaction between material surfaces and mucus at a molecular level, we grafted brushes of poly(2-methacryloyloxyethyl phosphorylcholine) (PMPC) followed by a straightforward installation of 3-phenylboronic acid (APBA) on silicon wafers. With the results obtained from our study, we expect to gain basic knowledge of the interactions between the zwitterionic polymer and the boronic acid APBA with mucin, which will be the basis for the chemical modification of particle surfaces with the purpose of improving their permeability through mucus.

EXPERIMENTAL

Materials

All chemicals and solvents were commercially available from Fisher Scientific, TCI, and Sigma Aldrich, and were used as received unless otherwise noted. Silicon wafers with front side polished/backside etched were obtained from International Wafer Service (stock lot #15145) with a diameter of 150 mm, a resistivity of 14-25 Ωcm and a thickness of 600-700 μm. Prior to surface modification, the wafers were cut into 1.0 cm × 1.0 cm squares using a diamond cutter on the etched side. 3-Aminopropyltriethoxysilane (APTES) was obtained from Oakwood Chemicals and used without further purification. The monomer, 2-methacryloyloxyethyl phosphorylcholine (MPC), and 3-(pen-4-ynamido)phenyl boronic acid were purchased from Ambeed and used without further purification. Non-functionalized silica nanoparticles with a mean diameter of 180 nm (lot number 14653) were purchased from Bangs Laboratories Inc. Nanopure water was treated with a Barnstead Nanopure system to a final resistance of 18.2 MW. Mucin from porcine stomach type II was purchased from Millipore Sigma. Prior to use, the mucin was purified by suspending it in nanopure water at a 2% w/v concentration. Then, the suspension was

centrifuged at 8000 rpm for 30 min at room temperature. The supernatant was collected and lyophilized for 72 hours. Fresh solutions of 2% w/v mucin in the corresponding buffer were prepared shortly before conducting experiments.

Pretreatment of silicon wafers

Silicon wafers squares were mounted on a custom-made wafer holder and submerged in a tube containing a freshly prepared solution of Alnochromix in concentrated sulfuric acid (6.97 g in 200 mL). The wafers were left to soak overnight, followed by rinsing with water (3 × 10 mL). Finally, they were dried under a stream of argon. After these treatments, the wafers were ready for silanization. Eight silicon wafers were mounted on the holder for each batch.

Surface modification of silicon wafers with an ATRP initiator

Clean silicon wafers were mounted on a custom-built wafer holder and placed in a dry flask with 25 mL of anhydrous toluene. Then, 65 μL (0.2 mmol) of (3-trimethoxysilyl)propyl 2-bromo-2-methylpropionate (silane ATRP) were added, and the mixture was stirred at room temperature overnight.[72] After this period, the wafers were removed from the silane solution and rinsed with toluene (3 × 10 mL) followed by methanol (3 × 10 mL). Finally, the wafers were dried under a stream of argon.

PMPC grafting from silicon wafers surface via SI-ARGET ATRP (SiW–PMPC)

Silanized silicon wafers were placed in a solution containing MPC (2000 mg, 6.77 mmol), ascorbic acid (11.93 mg, 0.007 mmol) and TPMA (19.67 mg, 0.007 mmol) in 20 mL of methanol. Then, (3-trimethoxysilyl)propyl 2-bromo-2-methylpropionate (2.25 mL, 0.008 mmol) was added to the solution to to carry out the characterization of the grafted polymer as it can be traced from the free initiator. The flask was sealed with a septum and the solution was stirred and bubbled

with argon for 30 min. Separately, a 10 mg/mL stock solution of copper bromide (II) in methanol was prepared and bubbled with argon for 30 min. After this time, 151 μL (0.0007 mmol) of copper bromide (II) solution was added to the flask containing the wafers. The polymerization was carried out at room temperature under argon for 18 h. After this time, the silicon wafers were removed from the mixture and rinsed with methanol (3 × 10 mL) and water (3 × 10 mL) and dried under a stream of argon.

Conjugation of boronic acid via click chemistry on silicon wafers (SiW–APBA)

PMPC-modified silicon wafers were azidolyzed by introducing them in a Schlenk tube with a solution of sodium azide in methanol (1 M) overnight. Then, the azide-terminated wafers were placed in a flask containing 3-(pen-4-ynamido)phenyl boronic acid (APBA) (65.7 mg, 0.3 mmol) and ascorbic acid (35.22 mg, 0.2 mmol) in 20 mL of methanol. The flask was capped with a rubber septum and bubbled with argon for 30 min. Separately, a 1 mg/mL stock solution of copper sulfate in methanol was prepared and bubbled with argon for 30 min. After both solutions were degassed, 0.998 mL (0.04 mmol) of the copper solution was added to the flask containing the wafers. The mixture was stirred at room temperature overnight. The wafers were then washed with a 0.1 M *N*,*N*-diethyldithiocarbamate sodium in methanol (3 × 10 mL) and then methanol (3 × 10 mL) to remove the excess of copper on the surface. Finally, the wafers were dried under a stream of argon.

Synthesis of amino-terminated silica nanoparticles with APTES (SiNP–NH_2)

Nominal 180 nm silica nanoparticles (2 mL of a 10% w/v suspension, 200 mg silica particles) were silanized with APTES as previously described.[2] Briefly, silica particles were transferred into anhydrous methanol by three cycles of centrifugation (13,000 rpm, 5 min) and redispersed using a combination of vortex mixing and sonication at room temperature. The nanoparticles were then dispersed in 10 mL of anhydrous toluene in a round-bottom flask equipped with a septum and a

magnetic stir bar, and sonicated for 30 min to achieve a homogeneous suspension. Following this, 205 μL (0.88 mmol) of APTES was added, and the suspension was sonicated for an additional 30 min. The mixture was then transferred to a constant-temperature bath at 90 °C and stirred overnight. Nanoparticle purification involved sequential centrifugation (13,000 rpm for 5 min) followed by redispersion using vortex mixing and sonication at room temperature with methanol and water (repeated five times for each solvent). Finally, the nanoparticles were dried under vacuum overnight to remove any residual water.

Conjugation of ATRP initiator onto silica nanoparticles (SiNP–Br)

Amino-terminated silica nanoparticles (SiNP–NH_2, 0.2 g) were dispersed in 10 mL of THF in a round bottom flask by sonication for 30 min to obtain a homogeneous suspension. Then, triethylamine (2.5 mL, 17.5 mmol) was added to the suspension, and the flask was placed in an ice-water bath. Next, 2-bromoisobutyryl bromide (2.2 mL, 17.5 mmol) was added dropwise to this suspension over 30 min. The reaction mixture was allowed to warm up to room temperature and stirred overnight. After the reaction was completed, the mixture was transferred to centrifuge tubes and centrifuged at 13,000 rpm for 5 min to isolate the nanoparticles. Purification involved sequential centrifugation (13,000 rpm for 5 min) followed by redispersion using vortex mixing and sonication at room temperature with methanol and water (three times per solvent). Finally, the particles were dried under vacuum overnight to remove any residual water.

Synthesis of PMPC-grafted nanoparticles via SI-ARGET ATRP (SiNP–PMPC)

Modified silica nanoparticles containing an ATRP initiator (SiNP-Br) were placed in a round bottom flask and dispersed in 15 mL of methanol using sonication. Then, MPC (2.3 g, 8 mmol), ascorbic acid (2.8 mg, 0.02 mmol) and tris(2-pyridylmethyl)amine (TPMA) (4.6 mg, 0.02 mmol) were added to the nanoparticle suspension. This mixture was stirred and bubbled with argon for 30 min. In a separate flask, a stock solution of copper bromide (II) in methanol (10 mg/mL) was prepared and bubbled with argon for 30 min. Once the nanoparticle suspension and the copper solution were bubbled, 35.7 mL (0.002 mmol) of copper bromide (II) solution was added to the flask containing the reaction mixture. Polymerization was carried out at room temperature under an argon atmosphere overnight. The polymerization was quenched by exposure to air and the mixture was cooled in an ice-water bath. The resulting nanoparticles (SiNP-PMPC) were purified

through sequential centrifugation (13,000 rpm for 5 min) followed by redispersion using vortex mixing and sonication at room temperature with methanol and water (three times per solvent). Finally, the particles were dried under vacuum overnight to remove any residual water.

Synthesis of boronic acid-terminated silica nanoparticles via click chemistry (SiNP–APBA)

Polymer-grafted silica nanoparticles SiNP–PMPC (0.2 g) were azidolyzed by introduction in a round bottom flask containing 15 mL of a 1 M solution of sodium azide in methanol and reacted overnight at room temperature. Purification involved centrifugation (13,000 rpm for 5 min) and redispersion at room temperature with a vortex/sonication combination with methanol (3×). Azide-terminated nanoparticles were placed in a round bottom flask containing 3-(pen-4-ynamido)phenyl boronic acid (APBA) (17.5 mg, 0.08 mmol) and ascorbic acid (9.39 mg, 0.05 mmol) in 10 mL of methanol. The suspension was bubbled with argon for 30 min. Separately, a 10 mg/mL stock solution of copper sulfate in methanol was prepared and bubbled with argon for 30 min. Then, 266 mL (0.02 mmol) of the copper solution were added to the flask containing the suspension. The reaction was allowed to proceed at room temperature overnight with constant stirring. The boronic acid modified particles were purified by centrifugation (13,000 rpm for 5 min) and redispersion with 0.1 M solution of *N*,*N*-diethyldithiocarbamate sodium in methanol (2 ×) and methanol (3 ×) via vortex mixing and sonication. Rinsed particles were dried under vacuum overnight.

Characterization methods

The surface composition of silicon wafers and silica nanoparticle was determined by X-ray photoelectron spectroscopy (XPS) on a PHI physical electronics PE-5800 X-ray photoelectron spectrometer with Al K_a X-ray source (1486.6 eV) and a takeoff angle of 45° (equivalent to a

penetration depth of 10 nm). The weight average molecular weight (M_w) and polydispersity (PDI) of the polymer were determined through the use of an initiator in solution to enable the analysis of free polymer. Size exclusion chromatography was carried out using a Waters 1515 Isocratic HPLC. Three PSS PFG linear M columns (300 mm × 8 mm) were connected in series and differential refractive index detector (Waters 2414) was used. The eluent (50 mM sodium trifluoroacetate in trifluoroethanol) was set at a flow rate of 1 mL/min and the temperature was held at 40 °C. A poly(methyl methacrylate) high calibration kit (PSS–mmkith) –including individual poly(methyl methacrylate) molecular mass standards with nominal M_p of 602–3,060,000 Da– was used to calibrate the system prior sample analysis. Before injection, samples were filtered through 0.45 μm hydrophilic PVDF filters. The thickness of the PMPC polymers on silicon wafers surface was obtained with a J.A. Wollan ellipsometer operating with a 632 nm laser at 70° incident angle from a range between 500 to 1000 nm under ambient conditions. Ellipsometric data obtained were fitted to a model of a PMPC layer of variable thickness on a silicon substrate using WVASE32 software. The model describes the refractive index using the Cauchy approximation ($RI = A_n+B_n/l^2$) with $A_n = 1.4778$ and $B_n = 0.004775$ mm^2. Fluorescence microscopy images of silicon wafers were taken with a fluorescence microscope (E-600, Nikon) with a 475 nm wavelength. To quantify the maximum fluorescence intensity of each APBA wafer, micrographs were analyzed with ImageJ software. Hydrodynamic diameter measurements of silica nanoparticles were performed on a Malvern Instruments Nano-ZS ZetaSizer using Nanopure water as solvent at a concentration of 1 mg/mL. Thermogravimetric analysis (TGA) of silica nanoparticles was carried out on a TA Q500 Thermogravimetric analyzer. Samples were heated from 30 °C to 800 °C at a 10 °C/min rate under a nitrogen atmosphere. Attenuated total reflection (ATR) infrared spectra were collected on a Thermo Nicolet iS-50 FTIR spectrometer on an ATR diamond. Alizarin red S (ARS) experiments were carried out on an Edinburgh FS5 spectrofluorometer. ARS solutions were prepared at a concentration of 1μM in Nanopure water. Silica nanoparticle suspensions of –PMPC and –APBA were prepared at a concentration of 1 mg/mL in Nanopure water. ARS solution (1 mL) and nanoparticle suspension (1 mL) were mixed for 25 min at room temperature in a clean scintillation vial and transferred to

a cuvette to then measure their fluorescence intensity at 575 nm with an excitation wavelength of 470 nm.

RESULTS AND DISCUSSION

Surface modification of silicon wafers

Silicon wafers were functionalized with (3-methoxysilyl)propyl 2-bromo-2-methylpropionate (silane-ATRP) to act as the surface-grafted ATRP initiator. Then, SI-ARGET ATRP was carried out to polymerize MPC from the surface, targeting 80 repeat units for consistency with our previous studies on zwitterionic analogues of Pluronic copolymers.[73–75] The molecular weight and PDI of the polymer were determined through the use of an initiator in solution to enable the analysis of free polymer.[76,77] Azidolysis was carried out post-polymerization by submerging treated silicon wafers in a solution of sodium azide to finally react it with 3-(pen-4-ynamido)phenyl boronic acid (APBA) for conjugation via an azide-alkyne "*click*" reaction (**Fig. 1**). A copper chelator (0.1 M *N*,*N*-diethyldithiocarbamate sodium in methanol) was used to remove excess copper from the wafer surface, as previously reported.[78]

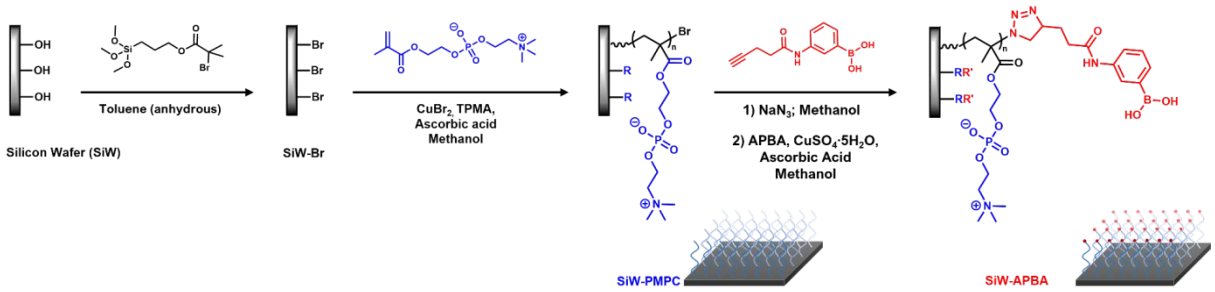

Fig. 1. Schematic representation of the modification of silicon wafer surfaces with an ATRP initiator (SiW-Br), followed by polymerization of MPC (SiW-PMPC), and finally end-group modification with aminophenyl boronic acid (SiW-APBA).

The molecular weight of grafted PMPC brushes was determined by analyzing the free polymer in solution since it has been reported that these have similar values.[79–81] MPC conversion reached 96% (77 repeat units or 22,715 g/mol) after 18 h, with a polydispersity of 1.10 (**Fig. S1**). Kinetic plots of the MPC polymerization showing the characteristic behavior of a controlled reaction are also included in **Fig. S1**. PMPC brush thickness was determined by ellipsometry. The thickness of

the silicon oxide layer and grafted ATRP initiator were measured and fit using the WVASE32 software (J.A. Woolam Co.),[82] and corresponded to 2.00 ± 0.002 nm.[83,84] The polymer-grafted wafer was then measured and the contribution of the initiator was subtracted from the final value. The thickness of the dry polymer layer was found to be 6.20 ± 0.01 nm. The silicon wafer with APBA was also measured to determine if the thickness of the polymer was conserved after end group modification. Using the same parameters as before, the thickness for SiW-APBA was 6.27 ± 0.01 nm, confirming that the polymer thickness remained constant after installation of the boronic acid.

The surface composition of silicon wafers after each modification step was determined by X-ray photoelectron spectroscopy (XPS) with a Al Kα X-ray source and a takeoff angle of 45°, which corresponds to a depth of analysis typically in the range of 5 to 10 nm from the outermost surface.[85] The elemental percentages based on the XPS analysis for silicon wafers at different modification stages are reported in **Table 1**.

Table 1. Elemental surface composition of silicon wafers at different stages of the surface modification process, obtained by XPS.

	B_{1s}	C_{1s}	N_{1s}	O_{1s}	Si_{2p}	P_{2p}	Br_{3d}	N/P
SiW-Br		22.57		52.07	25.36		8.62	
SiW-PMPC		60.84	5.01	29.03		5.12	1.04	0.97
SiW-APBA	0.27	59.06	5.42	29.09		5.09		1.06

The high-resolution carbon spectra for SiW–ATRP, SiW–PMPC, and SiW–APBA (**Fig. S2**, first column) showed the deconvolution of signals corresponding to the characteristic bonds present in each sample. In all cases, a peak around 285 eV is observed, corresponding to C-C and C-H bonds. Additionally, a shoulder appears in the range of 288-290 eV, which is associated with the ester group present both in the initiator (SiW–ATRP) and on the surfaces modified with PMPC. Upon analyzing this signal, it is observed that the percentage of this contribution increases for the polymer-modified surfaces, due to the presence of the ester derived from the methacrylate of MPC. MPC polymerization is also accompanied by the appearance of characteristic N_{1s} and P_{2p} signals, which are present in a N/P ratio of 0.97, in agreement with the theoretical ratio of 1. [86,87]

While the P_{2p} peak is the primary signal for identifying phosphorus in the sample, the P_{2s} peak can also be detected at a higher binding energy (typically around 190–200 eV), though with lower intensity. In contrast, the main boron peak, B_{1s}, is usually found in the same region, within a range of 187 to 193 eV.[85] Therefore, when analyzing the SiW–APBA samples to confirm the presence of boronic acid, it is observed that the main boron peak (B_{1s}) overlaps with the secondary phosphorus peak (P_{2s}). High-resolution spectra of the P_{2s} region of SiW–PMPC and SiW–APBA surfaces were compared to corroborate the success of the *click* reaction (**Fig. 2A**). As shown, the P_{2s} signal of SiW–PMPC was well fit with a single peak. In contrast, the high-resolution spectrum of this region for SiW–APBA (**Fig. 2B**) showed two peaks, the larger of which corresponded to the secondary peak of phosphorus (P_{2s}, 194 eV) that overlaps with primary signal of boron, which appears as a small shoulder at slightly lower binding energy (B_{1s}, 191 eV), thus confirming the presence of the boronic acid end group.

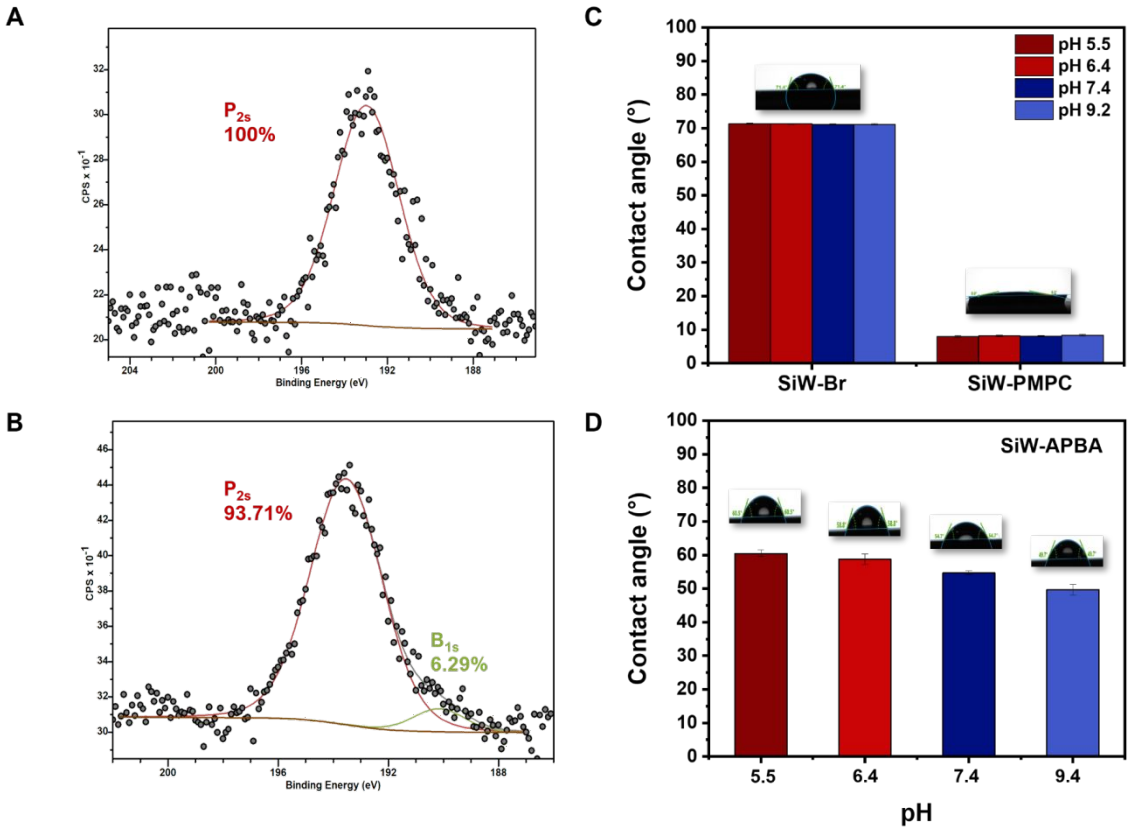

Fig. 2. P_{2s} high-resolution XPS spectra of SiW–PMPC (**A**) and SiW–APBA (**B**) showing the overlapped peak of B_{1s}, corresponding to the conjugated boronic acid. Contact angle for SiW-Br and SiW-PMPC (**C**)

and SiW-APBA (**D**) probed with buffers ranging from pH 5.5 to 9.2 to examine the surface hydrophilicity as function of pH. Error bars were determined from multiple measurements of contact angles on the corresponding wafer.

The surface hydrophilicity of SiW–Br, SiW–PMPC, and SiW–APBA wafers was determined by measuring the contact angle using nanopure water as the probe fluid (**Fig. 2C-D** at pH 6.4). The contact angle of SiW–Br was 71°±1°, indicating a hydrophobic surface after the silanization step. In contrast, the contact angle of the SiW–PMPC surface was 8°±1°, which is expected due to the hydrophilic properties of the polymer.[88] However, after the click reaction with APBA, the contact angle increased to 59°±2°. As previously mentioned, boronic acids coexist between a neutral and an anionic form in aqueous solution. The pK_a of boronic acids is the value where half of the boron centers exist as the anionic boronate species.[28] The reported pK_a value for APBA is 8.6, therefore, in nanopure water most of the boronic acids are expected to exist in the neutral form, which is more hydrophobic than PMPC, therefore an increase in the contact angle after installation of the boronic acid is reasonable.[36,89]

To study the effect of pH on surface hydrophilicity, contact angles for SiW–Br, SiW–PMPC, and SiW–APBA wafers were measured with buffered solutions at pH 5.5, 7.4, and 9.2 (10 μL drop measurements) (**Fig. 2C** and **2D**). Since the boronic acid is expected to exist mostly as a neutral species at pH values lower than its pK_a and in its anionic form at pH values higher than its pK_a, this pH range allows us to analyze the change in surface hydrophilicity with APBA. In the presence of the boronate anion, the surface is expected to be more hydrophilic and therefore the contact angle is expected to be lower.

Despite differences in the pH of the probe fluid, SiW–Br and SiW–PMPC wafers did not show any change in contact angle and remained at ~71° and ~8°, respectively. Conversely, APBA-modified wafers showed some sensitivity to the different buffers. For pH 5.5 and 6.4 the value obtained was ~ 60°; in these cases, most of the boronic acids are expected to be present in their neutral form. On the other hand, the contact angle decreased as the pH increased from 7.4 to 9.2, and the lowest value was observed at the latter pH (50°). These preliminary results indicate a slight sensitivity of the functional group to the pH of the environment.

Interaction studies of surface-modified silicon wafers with mucin

Previous reports discussed the preparation of well-defined PMPC brushes on silicon wafers and examined the effect of their surface properties on protein adsorption and cell adhesion.[83,89] However, to the best of our knowledge, there is no study focused on the surface interactions of PMPC-APBA and mucin. Thus, following the idea of protein adsorption to surfaces, chemically-modified silicon wafers were exposed to mucin solutions under different medium pH to study their interaction via labeling the available sialic acids, an abundant component of mucus, with wheat germ agglutinin (WGA).[90,91]

Kataoka and his group analyzed the binding profile of 3-(propionamido)phenylboronic acid (PAPBA) with *N*-acetylneuraminic acid (Neu5Ac, the predominant sialic acid found in human cells) in aqueous solutions varying the pH.[92] Interestingly, they found that the equilibrium constant for Neu5Ac binding to PAPBA gradually decreased by increasing the pH from 4 to 10, suggesting that, unlike other sugars, the neutral ester complex with the nonionic boronic acid is favored by Neu5Ac at lower pH. This effect was attributed to stabilization of the boronic acid $B(OH)_2$ complex with a glycerine moiety within Neu5Ac though intramolecular B-N and B-O interactions. Thus, buffered mucin solutions (2% wt) within the pH range examined by Kataoka (i.e., pH 5.5, 7.4, and 9.2) were used for adsorption experiments. SiW-PMPC and SiW-APBA were incubated in these solutions overnight and rinsed, and the surface-bound mucin was subsequently labeled with Alexa 488-labeled wheat germ agglutinin (AF488-WGA, 0.01 mg/mL) and imaged under a fluorescence microscope (E-600, Nikon) at a wavelength of 475 nm.

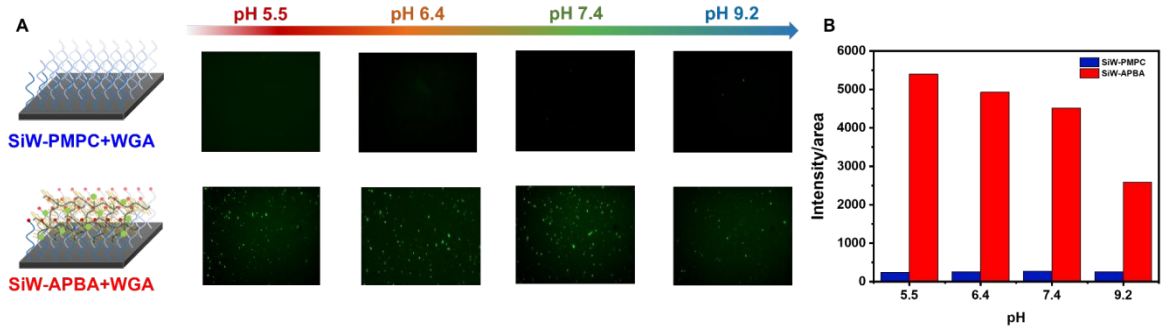

Fig. 3. (**A**) Schematic of the adsorption of AF488-WGA (shown in green) to PMPC and APBA surfaces. (**B**) Fluorescence micrographs of mucin-WGA adsorption on SiW-PMPC and SiW-APBA wafers in different buffer solutions. Images were obtained with an excitation wavelength of 475 nm at a magnification of 10×. (**C**) Comparison of fluorescence intensity per area for SiW-PMPC and SiW-APBA wafers under different pH conditions confirming the surface interaction between the boronic acid

and mucin.

As shown in **Fig. 3**, no fluorescence was detected for SiW–PMPC surfaces regardless of solution pH, suggesting that mucin did not adsorb because of a lack of agglutinin-binding functionalities. In contrast, all SiW–APBA samples showed fluorescence under the same conditions as a result of the sialic acid groups in mucin interacting with the boronic acids on the silicon wafer. When the samples are exposed to AF488-WGA, the free sialic acids remaining on mucin interact with the protein and fluorescence is observed. As shown, the fluorescence intensity varied inversely with buffer pH, as expected from Kataoka's findings.

Synthesis and characterization of surface-modified silica nanoparticles

Boronic acid-decorated silica nanoparticles (180 nm nominal diameter) were surface-modified following the four-step method illustrated in **Fig. 4**, which is a modification to that used for the functionalization of silicon wafers. Briefly, silica nanoparticles were initially silanized with (3-aminopropyl)triethoxysilane (APTES) to install surface amine moieties for conjugation with 2–bromoisobutyryl bromide. Once the initiator was conjugated, the monomer (MPC), was polymerized by SI-ARGET ATRP targeting ~80 repeat units, as before. The terminal bromine was then reacted with sodium azide to install 3-phenylboronic acid (APBA) via azide-alkyne cycloaddition.

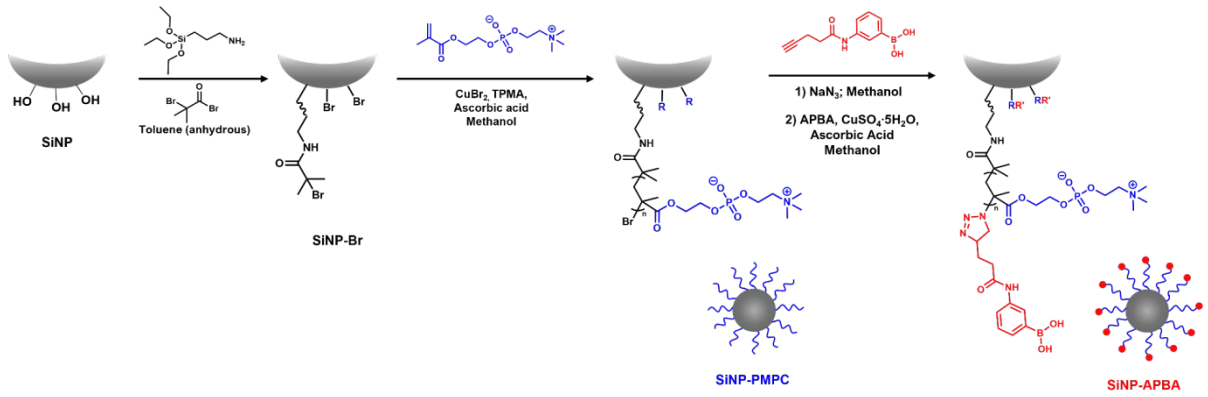

Fig. 4. Surface modification of silica nanoparticles. Installation of the ATRP initiator was carried out in two steps, starting with silanization with aminopropyltriethoxysilane, followed by coupling with 2-bromoisobutyrylbromide. Subsequently, PMPC polymerized by SI-ARGET ATRP. Azidolysis of the terminal bromine allowed for installation of the boronic acid *via* azide-alkyne cycloaddition.

The surface composition of silica nanoparticles after each modification step was also assessed by X-ray photoelectron spectroscopy (XPS) at a take-off angle of 45°. A comparison of the survey spectra of SiNP–Br, SiNP–PMPC and SiNP–APBA nanoparticles is provided in **Fig. 5A**, and the elemental composition is presented in **Table S1**. Characteristic peaks for C_{1s}, O_{1s}, N_{1s}, Si_{2p}, and Br_{3d} were observed after silanization with APTES and conjugation of the ATRP initiator. The N/Br ratio was estimated to be 1.03, suggesting a quantitative conjugation of the initiator. PMPC-grafted surfaces showed the expected signals for N_{1s} and P_{2p} with a N/P ratio of 1.08. In addition, the absence of the Si_{2p} peak is indicative of a PMPC layer thicker than 10 nm, which is the thickness probed at a 45° take-off angle. The high-resolution spectrum of the N_{1s} signal after PMPC grafting (**Fig. S3**) was deconvoluted into two peaks, the larger of which corresponds to the quaternary

amine characteristic of the phosphorylcholine group (~404 eV, 74%), whereas the smaller signal (~403 eV, 26%) was attributed to several functional moieties including C-N, triazoles, and amide groups of both PMPC and the conjugated boronic acid. After conjugation, the N/P ratio increased slightly from 1.08 to 1.11 due to the triazole ring and the amide group of the boronic acid. These results are consistent with previous reports.[93] FTIR analysis of silica nanoparticles (**Fig. S4A**) effectively showed the signals characteristic of the different functional groups of PMPC, however it was unable to detect signals attributed to the cycloaddition of the boronic acid moiety.

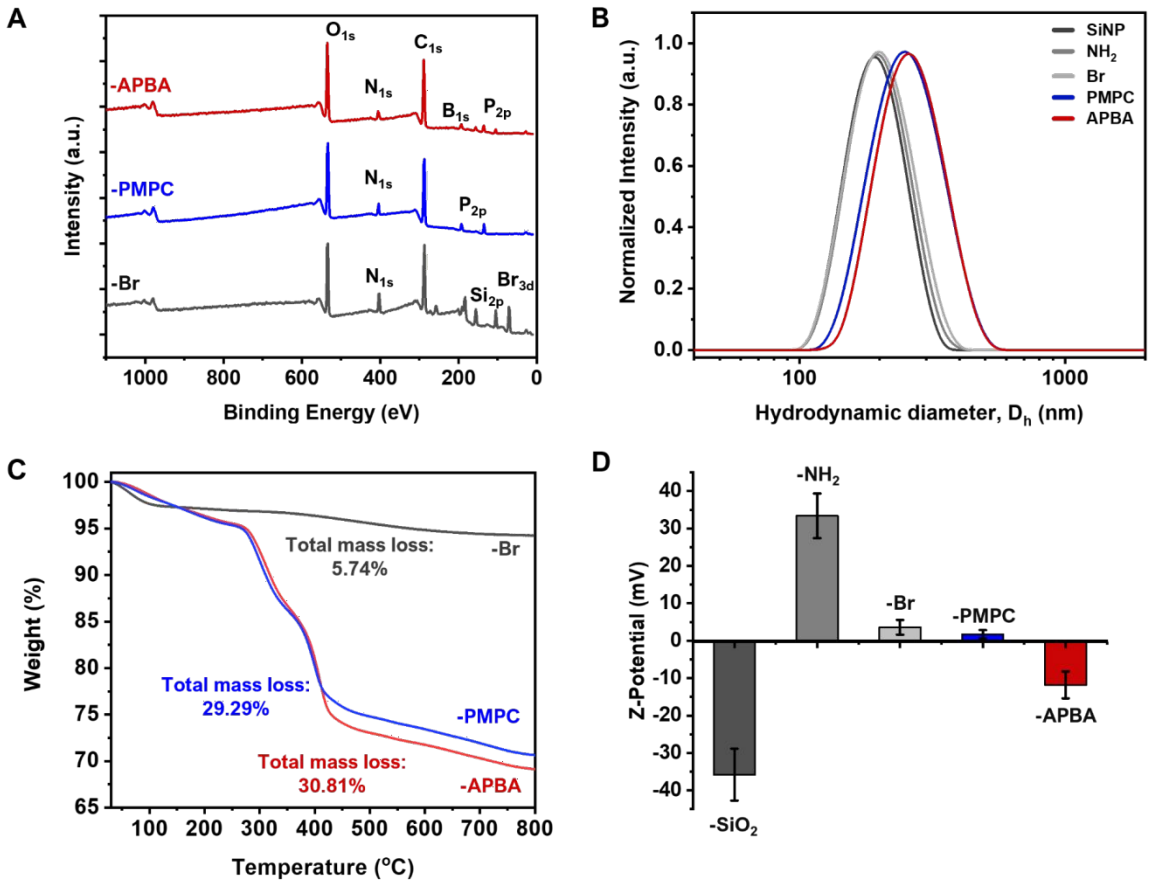

Fig. 5. Characterization of surface-modified silica nanoparticles. (**A**) XPS survey spectra of SiNP–Br, SiNP–PMPC, and SiNP–APBA showing the characteristic elements following each reaction step. (**B**) Hydrodynamic diameter of silica nanoparticles with different surface chemistries showing a major shift upon PMPC grafting. (**C**) Thermogravimetric analysis (10 K/min, in N_2) of SiNP–Br, SiNP–PMPC, and SiNP–APBA demonstrating that the significant mass loss noted is mainly due to the PMPC layer. (**D**) Zeta potential measurements showing the net neutrality of –PMPC surfaces, and the slight negative charge of the –APBA surface.

Modifications to nanoparticle surface chemistry were also tracked by changes in hydrodynamic size with DLS measurements in nanopure water (**Fig. 5B**). Unmodified SiO_2 nanoparticles had an initial diameter of 187.1 nm. After silanization, the size increased slightly to 192.4 nm and upon conjugation of the ATRP initiator their size increased once again to 195.7 nm. The major difference was observed after MPC polymerization, resulting in a diameter of 243.5 nm. Finally, the boronic acid-terminated particles showed a diameter of 253.8 nm. The polydispersity of all samples was low, with values ranging from 0.04 to 0.06. The estimated thickness of the PMPC coating on silica nanoparticles was considerably larger than that measured for silicon wafers, which we attribute to the fact that the latter was measured in the dry state.

Thermogravimetric analyses of silica nanoparticles with different surface chemistries were also carried out (**Fig. 5C**). The thermogram for SiNP–Br particles showed an overall mass loss of 5.74%, with an initial loss of adsorbed water (< 200 °C); decomposition of the organic layer on the surface was observed after 295 °C. The thermograms for SiNP–PMPC and SiNP–APBA showed a similar behavior, however the second mass loss (30.81% wt after 300 °C) was considerably more pronounced than in the case of SiNP–Br particles. The residual mass corresponds to the remaining inorganic SiO_2. Since the mass loss for SiNP–APBA particles is not significantly different to the mass loss of SiNP–PMPC particles, we can attribute these results primarily to decomposition of the PMPC layer during the analysis.

Surface charge was also tracked by measuring the zeta potential of nanoparticles in water at different stages of modification (**Fig. 5D**). A dramatic change from -38 mV to 31 mV was observed after silanization, consistent with the change from surface silanols to amino groups. Conjugation of the ATRP initiator reduced the charge to 3.6 mV and grafting of the PMPC layer lowered this value to 1.5 mV, resulting in a primarily neutral surface change. The cycloaddition of APBA further reduced the zeta potential to -10 mV, consistent with some of the boronic acids existing in the anionic form. Overall, these results are congruent with previous reports.[94–96]

Further confirmation of the presence of boronic acids on the surfaces of –APBA samples was obtained from an Alizarin Red S (ARS) assay. ARS is a hydrophilic catechol-containing dye that can complex to boronic acids; fluorescence is only observed upon conjugation. As shown in **Fig. S4**, the fluorescence emission spectra of ARS (as reference) and –PMPC particles incubated in ARS showed that both species are non-fluorescent. On the other hand, –APBA particles that were

incubated in a solution containing ARS showed a significantly higher emission, thus confirming the presence of the boronic acid moiety. The fluorescence intensity of –APBA particles was used to estimate the concentration of functional groups on the surface, which corresponded to 0.15 APBA moieties/nm^2, or 3.75x10^{-9} mol of APBA/mg sample.

Colloidal stability of SiNP–PMPC and SiNP–APBA in mucin solutions

The colloidal stability of SiNP–PMPC and SiNP–ABPA samples was tracked by DLS at different mucin concentrations and pH (**Fig. 6**). For this, NP suspensions were incubated in 2% wt porcine type II mucin at 37 °C in buffers at pH 3.0, 5.4 and 7.4. The shift to probing nanoparticle colloidal stability toward more acidic conditions (i.e., pH 3.0) was in response to the results obtained from the silicon wafer experiments, which showed a stronger interaction at lower pH. The changes observed are discussed in terms of sialic acid:end-group (SA:EG) molar ratios, which ranged between 100:1 to 1:100 (or 100 and 0.01, respectively). End-group concentration was extracted from an estimate concentration of functional groups on the surface results after the ARS test mentioned above, whereas the concentration of sialic acids was assumed to be 1.2% wt based on the value reported for porcine stomach mucin type II, as per the source (Millipore Sigma). Size distributions and autocorrelation functions of SiNP–APBA samples are reported in **Fig. S6**.

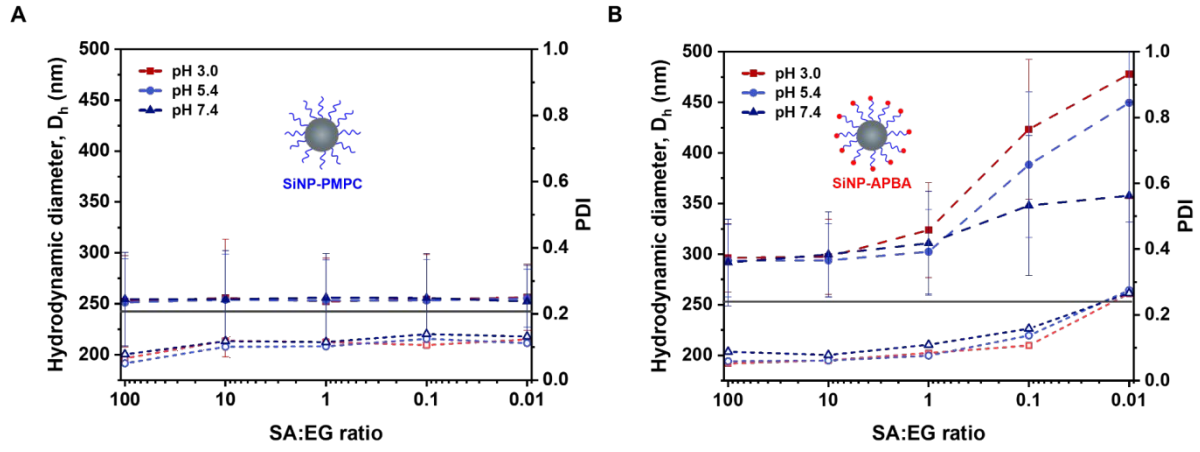

Fig. 6. Hydrodynamic size of PMPC- and APBA-modified silica nanoparticles incubated in mucin solutions at different sialic acid:end group ratios (SA:EG) under different pH, obtained by DLS. In both graphs, the solid horizontal dark gray line represents the original dimensions of the particles in DI water (i.e., prior to incubation). The squares indicate the data for pH 3.0, the circles for pH 5.4 and the triangles for pH 7.4. Filled symbols represent hydrodynamic diameter, whereas empty symbols correspond to polydispersity (PDI). (**A**) SiNP–PMPC samples showing no change in size or PDI regardless of the

amount of mucin present in the mixture. (**B**) SiNP–APBA samples exhibiting a pH- and SA:EG-dependent behavior, resulting from the interaction between boronic acids on NP surfaces and sialic acids on mucin.

As presented in **Fig. 6A**, PMPC-coated samples showed only a small increase in hydrodynamic diameter upon incubation in mucin (filled symbols vs. horizontal grey line), which was independent of system pH and SA:EG ratio, suggesting the absence of interactions between the zwitterionic polymer and mucin, in line with the observations made for SiW–PMPC (**Fig. 3**). Moreover, these samples showed no changes in size dispersity upon incubation. Given the negligible PMPC-mucin interaction, we attribute the apparent increase in hydrodynamic dimensions to a decrease in particle diffusion caused by the presence of mucin in the medium, since the hydrodynamic diameter obtained in DLS is related to the diffusion of the particles in the medium by the Stokes-Einstein equation (see Supporting Information). Further examination of the data at different pH revealed a small (~ 9 nm) yet consistent increase in hydrodynamic diameter with mucin concentration at a SA:EG ratio of 1:1 (**Fig. S5**). Therefore, we attribute the small increase in hydrodynamic diameter of SiNP–PMPC samples to the increase in the viscosity of the solution with mucin content, as previously reported.[97–100]

In contrast, SiNP–APBA samples showed a considerable increase in hydrodynamic dimensions in the presence of mucin, as clearly observed when comparing the filled symbols with the horizontal grey line in **Fig. 6B**. The increase –attributed primarily to boronic acid:sialic acid interactions– was sensitive not only to the SA:EG ratio, but also to system pH. Size distribution curves and the corresponding correlation functions for SiNP-APBA samples are provided in **Fig. S6**. All samples exhibited monomodal distributions and a rapid decay of the correlation function, characteristic of monodisperse samples, indicating that particle aggregation did not occur. These results suggest that the apparent increase in hydrodynamic diameter reflects decreased particle diffusion attributed to NP-mucin interactions. All samples show a similar trend regardless of system pH: sample polydispersity and hydrodynamic diameters are the lowest at the highest SA:EG ratios. This result could be explained by a combination of effects, including mucin adsorption onto nanoparticle surfaces, yielding an increase in particle size, and in a minor extent to the increase in medium viscosity, ultimately limiting nanoparticle diffusion in the mucin-rich medium. However, as the SA:EG ratio decreases from 1 to 0.01, polydispersity increases (0.1 to 0.3) and pH plays a stronger

role in mediating nanoparticle-mucin interaction, analogous to the behavior observed for the SiW–APBA/WGA system. Moreover, particle diffusion is increasingly hindered by mucin proteins within this mucin-deficient regime. As the pH of the solution decreases, nanoparticle-mucin interaction is increasingly favored and consequently the hydrodynamic diameter of the sample at pH 3.0 is the highest.

These results highlight the importance of designing particle surface chemistry with potential application in drug delivery, and specifically for transmucosal delivery. It is essential to establish surface interactions with mucus as this influences particle retention and penetration through this barrier. Furthermore, a relationship can be established between surface interactions and particle diffusion in biologically relevant fluids. With preliminary data such as those shown in this work, particle surface chemistry can be designed to not only establish the relevance of the interaction between particle and mucin, but also how it influences their diffusion.

It has been shown that the ratio between the functional groups that establish the interaction between nanoparticles and mucin is important to modulate their diffusion. Furthermore, the sensitivity shown by our system to the surrounding pH is also relevant since diffusion is modified according to how favored a specific interaction is at a certain pH. In this case, we observe that by decreasing the SA:BA ratio and increasing the pH, the interaction between the particles and mucin is favored but this slows particle diffusion. Therefore, these results may be a starting point for future work in which the design of the nanoparticle surface focuses on ensuring that the density of functional groups is adequate to allow an interaction with mucus that prolongs the residence time of the particles in mucus and prevents premature clearance without limiting their diffusion. It should be noted that pH sensitivity is also very important since the conditions of the medium will be determined by the type of mucus under study –which not only varies within the body but also between healthy and diseased states– so the relationship between the density of functional groups and the factors that favor their interaction with mucus at a certain pH will influence nanoparticle diffusion.

CONCLUSIONS

Silicon wafers and silica nanoparticles were successfully modified with PMPC brushes and APBA-termini through SI-ARGET ATRP and the cycloaddition of alkynyl-APBA, respectively. Boronic acid incorporation was confirmed by XPS and ARS assays. Differences in surface hydrophilicity between PMPC and APBA-modified silicon wafers were assessed by contact angle measurements using various buffer solutions as probe fluids, revealing that the wettability of boronic acid-functionalized surfaces is sensitive to environmental pH. Surface-modified silicon wafers were exposed to solutions of porcine gastric mucin (PGM) and the interaction between the terminal moieties and mucin was assessed by fluorescence microscopy via labeling with wheat germ agglutinin. The observed changes in hydrophilicity and mucus adsorption, influenced by pH variation, provided insight into the modulation of the mucoadhesive properties of the terminal boronic acid. Particle stability, assessed by DLS, corroborated the fluorescence microscopy results, showing that SiNP-PMPC exhibited no mucin interaction, while for SiNP-APBA the strength of boronic acid-sialic acid interaction dictated the change in diffusivity of the particles and therefore the hydrodynamic diameter measured. These results showed that by decreasing the SA:EG ratio and the pH, the interaction between the particles and mucin is favored, hindering particle diffusion. The findings shown here underscore the importance of surface chemistry in nanoparticle design, as they allow for modulation of particle-mucin interactions and at the same time influence the diffusion of particles in the medium. The relationship between functional groups on the particle surface and in mucin, as well as the pH of the system, were shown to be important in favoring certain types of interactions. This can be relevant for transmucosal delivery, since, depending on the type of mucus, the pH of the system can vary.

Data availability

The data supporting the information provided in this article has been included in the supporting information.

Conflicts of interest

There are no conflicts of interest to declare.

Acknowledgements

This project was sponsored by the National Science Foundation (NSF) project DMR/BMAT 2104498. The characterization of our materials was carried out at the Analytical Resources Core (ARC) at Colorado State University (RRID: SCR_021758). The authors acknowledge Professor Ramya Kumar and Adam Humpal at Colorado School of Mines for their help with ellipsometry measurements. We also thank Rahmi Lee at Colorado State University for her help with the fluorescence microscopy measurements.

REFERENCES

1 R. Bansil and B. S. Turner, *Adv. Drug Deliv. Rev.*, 2018, **124**, 3–15.
2 J. Watchorn, A. J. Clasky, G. Prakash, I. A. E. Johnston, P. Z. Chen and F. X. Gu, *ACS Biomater. Sci. Eng.*, 2022, **8**, 1396–1426.
3 R. A. Cone, *Adv. Drug Deliv. Rev.*, 2009, **61**, 75–85.
4 A. Popov, *J. Ocul. Pharmacol. Ther.*, 2020, **36**, 366–375.
5 P. H. Hamming, N. J. Overeem and J. Huskens, *Chem. Sci.*, 2020, **11**, 27–36.
6 D. Song, E. Iverson, L. Kaler, S. Bader, M. A. Scull and G. A. Duncan, *ACS Biomater. Sci. Eng.*, 2021, **7**, 2723–2733.
7 M. D. Vahey and D. A. Fletcher, *Elife*, , DOI:10.7554/eLife.43764.
8 L. Kaler, E. Iverson, S. Bader, D. Song, M. A. Scull and G. A. Duncan, *Commun. Biol.*, 2022, **5**, 249.
9 J. Y. Lock, T. L. Carlson and R. L. Carrier, *Adv. Drug Deliv. Rev.*, 2018, **124**, 34–49.
10 N. Martínez-Sáez, J. M. Peregrina and F. Corzana, *Chem. Soc. Rev.*, 2017, **46**, 7154–7175.
11 K. Joyner, D. Song, R. F. Hawkins, R. D. Silcott and G. A. Duncan, *Soft Matter*, 2019, **15**, 9632–9639.
12 J. K. W. Lam, C. C. K. Cheung, M. Y. T. Chow, E. Harrop, S. Lapwood, S. I. G. Barclay and I. C. K. Wong, *Adv. Drug Deliv. Rev.*, 2020, **160**, 234–243.
13 J. Mašek, D. Lubasová, R. Lukáč, P. Turánek-Knotigová, P. Kulich, J. Plocková, E. Mašková, L. Procházka, Š. Koudelka, N. Sasithorn, J. Gombos, E. Bartheldyová, F. Hubatka, M. Raška, A. D. Miller and J. Turánek, *J. Control. Release*, 2017, **249**, 183–195.
14 W. Shan, X. Zhu, M. Liu, L. Li, J. Zhong, W. Sun, Z. Zhang and Y. Huang, *ACS Nano*, 2015, **9**, 2345–2356.
15 V. V. Khutoryanskiy, *Adv. Drug Deliv. Rev.*, 2018, **124**, 140–149.
16 Q. Xu, L. M. Ensign, N. J. Boylan, A. Schön, X. Gong, J.-C. Yang, N. W. Lamb, S. Cai, T. Yu, E. Freire and J. Hanes, *ACS Nano*, 2015, **9**, 9217–9227.
17 K. Maisel, M. Reddy, Q. G. Xu, S. Chattopadhyay, R. Cone, L. M. Ensign and J. Hanes, *Nanomedicine (Lond.)*, 2016, **11**, 1337–1343.
18 C. S. Schneider, Q. Xu, N. J. Boylan, J. Chisholm, B. C. Tang, B. S. Schuster, A. Henning, L. M. Ensign, E. Lee, P. Adstamongkonkul, B. W. Simons, S.-Y. S. Wang, X. Gong, T. Yu, M. P. Boyle, J. S. Suk and J. Hanes, *Sci. Adv.*, 2017, **3**, e1601556–e1601556.
19 B. C. Tang, M. Dawson, S. K. Lai, Y. Y. Wang, J. S. Suk, M. Yang, P. Zeitlin, M. P. Boyle, J. Fu and J. Hanes, *Proc. Natl. Acad. Sci. U. S. A.*, 2009, **106**, 19268–19273.
20 Z. G. Estephan, P. S. Schlenoff and J. B. Schlenoff, *Langmuir*, 2011, **27**, 6794–6800.
21 M. Papi, D. Pozzi, V. Palmieri and G. Caracciolo, *Nano Today*, ,

DOI:10.1016/j.nantod.2022.101403.
22 D. Stengel, B. H. Demirel, P. Knoll, M. Truszkowska, F. Laffleur and A. Bernkop-Schnürch, *J. Colloid Interface Sci.*, 2023, **647**, 52–64.
23 L. Y. Zhou, Y. H. Zhu, X. Y. Wang, C. Shen, X. W. Wei, T. Xu and Z. Y. He, *Comput. Struct. Biotechnol. J.*, 2020, **18**, 1980–1999.
24 Z. P. Zeng, S. Chen and Y. M. Chen, *ChemMedChem*, , DOI:10.1002/cmdc.202300245.
25 E. Taipaleenm?ki, E. Brodszkij and B. St?dler, *ChemNanoMat*, 2020, **6**, 744–750.
26 X. Han, Y. Lu, J. Xie, E. Zhang, H. Zhu, H. Du, K. Wang, B. Song, C. Yang, Y. Shi and Z. Cao, *Nat. Nanotechnol.*, 2020, **15**, 605–614.
27 R. Rao, X. Liu, Y. Li, X. Tan, H. Zhou, X. Bai, X. Yang and W. Liu, *Biomater. Sci.*, 2021, **9**, 685–699.
28 Q. Li, C. Wen, J. Yang, X. Zhou, Y. Zhu, J. Zheng, G. Cheng, J. Bai, T. Xu, J. Ji, S. Jiang, L. Zhang and P. Zhang, *Chem. Rev.*, 2022, **122**, 17073–17154.
29 S. Moayedi, W. Xia, L. Lundergan, H. Yuan and J. Xu, *Langmuir*, 2024, **40**, 23125–23145.
30 M. Zhang, P. Yu, J. Xie and J. Li, *J. Mater. Chem. B Mater. Biol. Med.*, 2022, **10**, 2338–2356.
31 K. Qu, Z. Yuan, Y. Wang, Z. Song, X. Gong, Y. Zhao, Q. Mu, Q. Zhan, W. Xu and L. Wang, *ChemPhysMater*, 2022, **1**, 294–309.
32 Y. Li, W. Zhang, R. Zhao and X. Zhang, *Bioact. Mater.*, 2022, **15**, 392–408.
33 K. Liu, Y. Chen, Z. Yang and J. Jin, *Int. J. Biol. Macromol.*, 2023, **236**, 123870.
34 Y.-Y. Aung, A. N. Kristanti, H. V. Lee and M. Z. Fahmi, *ACS Omega*, 2021, **6**, 17750–17765.
35 W. Chen, X. Zhen, W. Wu and X. Jiang, *Sci. China Chem.*, 2020, **63**, 648–664.
36 W. L. A. Brooks and B. S. Sumerlin, *Chem. Rev.*, 2016, **116**, 1375–1397.
37 J. N. Cambre and B. S. Sumerlin, *Polymer (Guildf.)*, 2011, **52**, 4631–4643.
38 Y. Zhang, Y. Yu, G. Li, X. Zhang, Z. Wu and L. Lin, *J. Mater. Chem. B Mater. Biol. Med.*, 2021, **9**, 4190–4200.
39 A. Stubelius, S. Lee and A. Almutairi, *Acc. Chem. Res.*, 2019, **52**, 3108–3119.
40 G. Springsteen and B. H. Wang, *Tetrahedron*, 2002, **58**, 5291–5300.
41 D. G. Hall, *Boronic Acids: Preparation and Applications in Organic Synthesis and Medicine*, 2005, 1–99.
42 Y. Wang, Z. Chai, N. Wang, X. Ren and M. Gao, *J. Biomater. Sci. Polym. Ed.*, 2015, **26**, 617–628.
43 K. Oluwadamilola Miriam, I. A. Rosemary, I. W. Adebimpe, A. M. Olusola, P. Prasopchai, S. B. Olanrewaju and O. A. Adediran, *J. Drug Deliv. Sci. Technol.*, 2023, **87**, 104810.
44 M. H. Abu Elella and O. M. Kolawole, *Int. J. Biol. Macromol.*, 2024, **277**, 134531.
45 X. Wei, X. Duan, Y. Zhang, Z. Ma, C. Li and X. Zhang, *ACS Appl. Bio Mater.*, 2020, **3**, 2132–2139.
46 M. Surendranath, R. M. Ramesan, P. Nair and R. Parameswaran, *ACS Appl. Bio Mater.*, 2024, **7**, 7429–7443.
47 X. Zhang, G. Zhong, S. Peng, C. Zhang, B. Li, Z. Xia, Y. Zhu, G. Tao, R. Cai and X. Xu, *ACS Biomater. Sci. Eng.*, 2025, **11**, 1106–1122.
48 G. Prosperi-Porta, S. Kedzior, B. Muirhead and H. Sheardown, *Biomacromolecules*, 2016, **17**, 1449–1457.
49 K. Nagasaka, H. Komatsu, S. Ito, D. Palai, A. Nishiguchi and T. Taguchi, *Colloids Surf. B Biointerfaces*, 2025, **245**, 114307.

50 L. d'Amone, J. K. Sahoo, N. Ostrovsky-Snider, D. L. Kaplan and F. G. Omenetto, *Biomacromolecules*, 2023, **24**, 1310–1317.
51 C. Li, Z. Huang, Z. Liu, L. Ci, Z. Liu, Y. Liu, X. Yan and W. Lu, *IJN*, 2016, **11**, 5917–5930.
52 Y. Zhang, M. Li, B. Li and W. Sheng, *Langmuir*, 2024, **40**, 5571–5589.
53 T. Masuda and M. Takai, *J. Mater. Chem. B Mater. Biol. Med.*, 2022, **10**, 1473–1485.
54 M. Badoux, M. Billing and H.-A. Klok, *Polym. Chem.*, 2019, **10**, 2925–2951.
55 S. Dhingra, S. Sharma and S. Saha, *ACS Appl. Bio Mater.*, 2022, **5**, 1364–1390.
56 C. M. Hui, J. Pietrasik, M. Schmitt, C. Mahoney, J. Choi, M. R. Bockstaller and K. Matyjaszewski, *Chem. Mater.*, 2014, **26**, 745–762.
57 J. Qin, E. Ziemann, E. Bar-Zeev, S. E. Bone, Y. Liang, M. S. Mauter, M. Herzberg and R. Bernstein, *ACS Appl. Mater. Interfaces*, 2023, **15**, 18343–18353.
58 W. Feng, S. Zhu, K. Ishihara and J. L. Brash, *Langmuir*, 2005, **21**, 5980–5987.
59 K. Fukazawa, A. Nakao, M. Maeda and K. Ishihara, *ACS Appl. Mater. Interfaces*, 2016, **8**, 24994–24998.
60 Y. Inoue, Y. Onodera and K. Ishihara, *Colloids Surf. B Biointerfaces*, 2016, **141**, 507–512.
61 X. Hu, G. Szczepaniak, A. Lewandowska-Andralojc, J. Jeong, B. Li, H. Murata, R. Yin, A. M. Jazani, S. R. Das and K. Matyjaszewski, *J. Am. Chem. Soc.*, 2023, **145**, 24315–24327.
62 W. Yan, M. Fantin, S. Ramakrishna, N. D. Spencer, K. Matyjaszewski and E. M. Benetti, *ACS Appl. Mater. Interfaces*, 2019, **11**, 27470–27477.
63 J. O. Zoppe, N. C. Ataman, P. Mocny, J. Wang, J. Moraes and H.-A. Klok, *Chem. Rev.*, 2017, **117**, 1105–1318.
64 W. Jeong, H. Kang, E. Kim, J. Jeong and D. Hong, *Langmuir*, 2019, **35**, 13268–13274.
65 H. Kang, W. Jeong and D. Hong, *Langmuir*, 2019, **35**, 7744–7750.
66 *Miniemulsion ARGET ATRP via Interfacial and Ion-Pair Catalysis:From ppm to ppb of Residual Copper*, .
67 A. H. Agergaard, S. U. Pedersen, H. Birkedal and K. Daasbjerg, *Polym. Chem.*, 2020, **11**, 5572–5577.
68 A. Macior, I. Zaborniak, K. Wolski, K. Spilarewicz, J. Raczkowska, N. Janiszewska, K. Awsiuk and P. Chmielarz, *ACS Appl. Polym. Mater.*, , DOI:10.1021/acsapm.4c02034.
69 J. Jeong, H. Bisht, S. Park, Y. Hong, G. Shin and D. Hong, *Langmuir*, 2023, **39**, 7598–7604.
70 D. Hong, H.-C. Hung, K. Wu, X. Lin, F. Sun, P. Zhang, S. Liu, K. E. Cook and S. Jiang, *ACS Appl. Mater. Interfaces*, 2017, **9**, 9255–9259.
71 N. Li, T. Li, X.-Y. Qiao, R. Li, Y. Yao and Y.-K. Gong, *ACS Appl. Mater. Interfaces*, 2020, **12**, 12337–12344.
72 A. Pettignano, S. Grijalvo, M. Häring, R. Eritja, N. Tanchoux, F. Quignard and D. Díaz Díaz, *Chem. Commun. (Camb.)*, 2017, **53**, 3350–3353.
73 M. G. Petroff, E. A. Garcia, R. A. Dengler, M. Herrera-Alonso and M. A. Bevan, *Macromolecules*, 2018, **51**, 9156–9164.
74 M. G. Petroff, E. A. Garcia, M. Herrera-Alonso and M. A. Bevan, *Langmuir*, 2019, **35**, 4976–4985.
75 E. Jumai'an, E. Garcia, M. Herrera-Alonso and M. A. Bevan, *Macromolecules*, 2020, **53**, 9769–9778.
76 G. Xu, P. Liu, D. Pranantyo, L. Xu, K.-G. Neoh and E.-T. Kang, *Ind. Eng. Chem. Res.*, 2017, **56**, 14479–14488.

77 K. Ishihara, T. Kitagawa and Y. Inoue, *ACS Biomater. Sci. Eng.*, 2015, **1**, 103–109.
78 M. Kar, P. S. Vijayakumar, B. L. V. Prasad and S. Sen Gupta, *Langmuir*, 2010, **26**, 5772–5781.
79 C.-N. Yan, L. Xu, Q.-D. Liu, W. Zhang, R. Jia, C.-Z. Liu, S.-S. Wang, L.-P. Wang and G. Li, *Polymers (Basel)*, 2019, **11**, 1228.
80 J.-M. Moon, B.-S. Kim, H.-J. Paik, J.-O. Lee, E. Mouri and K. Yoshinaga, *Polym. Eng. Sci.*, 2010, **50**, 1067–1074.
81 J.-K. Chen, H.-Y. Huang, C.-W. Tu, L.-T. Lee, T. Jamnongkan and C.-F. Huang, *Polymers (Basel)*, 2022, **14**, 946.
82 R. Iwata, P. Suk-In, V. P. Hoven, A. Takahara, K. Akiyoshi and Y. Iwasaki, *Biomacromolecules*, 2004, **5**, 2308–2314.
83 Z. Zhang, A. J. Morse, S. P. Armes, A. L. Lewis, M. Geoghegan and G. J. Leggett, *Langmuir*, 2011, **27**, 2514–2521.
84 A. J. Morse, S. Edmondson, D. Dupin, S. P. Armes, Z. Zhang, G. J. Leggett, R. L. Thompson and A. L. Lewis, *Soft Matter*, 2010, **6**, 1571–1579.
85 J. E. Castle, *Surf. Interface Anal.*, 1984, **6**, 302–302.
86 M. Flejszar, P. Chmielarz, K. Wolski, G. Grześ and S. Zapotoczny, *Materials (Basel)*, 2020, **13**, 3559.
87 S. Feng, Y. Liu, J. Li and S. Wen, *Macromolecules*, 2021, **54**, 5719–5727.
88 L. Mao, X. Liu, M. Liu, L. Huang, D. Xu, R. Jiang, Q. Huang, Y. Wen, X. Zhang and Y. Wei, *Appl. Surf. Sci.*, 2017, **419**, 188–196.
89 A. N. Prossnitz and S. H. Pun, *ACS Macro Lett.*, 2022, **11**, 276–283.
90 W. Feng, J. Brash and S. Zhu, *J. Polym. Sci. A Polym. Chem.*, 2004, **42**, 2931–2942.
91 V. P. Bhavanandan and A. W. Katlic, *J. Biol. Chem.*, 1979, **254**, 4000–4008.
92 H. Otsuka, E. Uchimura, H. Koshino, T. Okano and K. Kataoka, *J. Am. Chem. Soc.*, 2003, **125**, 3493–3502.
93 Z. Liu and H. He, *Acc. Chem. Res.*, 2017, **50**, 2185–2193.
94 W. L. A. Brooks, C. C. Deng and B. S. Sumerlin, *ACS Omega*, 2018, **3**, 17863–17870.
95 H. Zheng, H. Gong, L. Cao, H. Lin and L. Ye, *Colloids Surf. B Biointerfaces*, 2021, **197**, 111433.
96 Z. Xu, K. M. A. Uddin, T. Kamra, J. Schnadt and L. Ye, *ACS Appl. Mater. Interfaces*, 2014, **6**, 1406–1414.
97 M. Ahmad, C. Ritzoulis and J. Chen, *Colloids Surf. B Biointerfaces*, 2018, **171**, 614–621.
98 J. Song, B. Winkeljann and O. Lieleg, *ACS Appl. Bio Mater.*, 2019, **2**, 3448–3457.
99 J. Zhang, Y. Lv, B. Wang, S. Zhao, M. Tan, G. Lv and X. Ma, *Mol. Pharm.*, 2015, **12**, 695–705.
100 H. Rulff, R. F. Schmidt, L.-F. Wei, K. Fentker, Y. Kerkhoff, P. Mertins, M. A. Mall, D. Lauster and M. Gradzielski, *Biomacromolecules*, 2024, **25**, 4014–4029.

Data availability

The data supporting the information provided in this article has been included in the supporting information.